

Strong coupling between weakly guided semiconductor nanowire modes and an organic dyeDiego R. Abujetas,¹ Johannes Feist,² Francisco J. García-Vidal,² Jaime Gómez Rivas,³ and José A. Sánchez-Gil¹¹*Instituto de Estructura de la Materia, Consejo Superior de Investigaciones Científicas, Serrano 121, 28006 Madrid, Spain*²*Departamento de Física Teórica de la Materia Condensada and Condensed Matter Physics Center, Universidad Autónoma de Madrid, 28049 Madrid, Spain*³*Institute for Photonic Integration, Department of Applied Physics, Eindhoven University of Technology, P.O. Box 513, 5600 MB Eindhoven, Netherlands*

(Received 2 April 2019; revised manuscript received 17 April 2019; published 9 May 2019)

The light-matter coupling between electromagnetic modes guided by a semiconductor nanowire and excitonic states of molecules localized in its surrounding media is studied from both classical and quantum perspectives, with the aim of describing the strong-coupling regime. Weakly guided modes (bare photonic modes) are found through a classical analysis, identifying those lowest-order modes presenting large electromagnetic fields spreading outside the nanowire while preserving their robust guided behavior. Experimental fits of the dielectric permittivity of an organic dye that exhibits excitonic states are used for realistic scenarios. A quantum model properly confirms through an avoided mode crossing that the strong-coupling regime can be achieved for this configuration, leading to Rabi splitting values above 100 meV. In addition, it is shown that the coupling strength depends on the fraction of energy spread outside the nanowire, rather than on the mode field localization. These results open up a new avenue towards strong-coupling phenomenology involving propagating modes in nonabsorbing media.

DOI: [10.1103/PhysRevB.99.205409](https://doi.org/10.1103/PhysRevB.99.205409)**I. INTRODUCTION**

Tailoring light-matter interaction at the nanoscale is the foundation to improve, beyond unpredictable limits, the efficiency of previous devices and to develop novel applications [1]. Among others, much effort has been undertaken to engineer the emission properties between electronic energy states of systems such as quantum dots, wells, and dye molecules, through the coupling to optical systems such as cavities, photonic crystals, metallic interfaces, and semiconductor wires [2–6]. Depending on the strength of the coupling between the systems two distinct regimes, weak and strong, can be established. In the weak regime, the spontaneous emission rate is strongly affected by the electromagnetic local densities of states, and it can be completely suppressed or enhanced by several orders of magnitude [7–10], but the natural frequency of the transition remains unaltered. Otherwise, the strong regime is characterized by a coherent exchange of energy between modes inducing new hybrid states with fascinating properties that can be very different from those of the initial systems [11–14].

Metallic nanostructures, through localized surface plasmons and surface plasmon polaritons, can effectively couple to electronic transition states due to their optical near-field enhancement and confinement [15–21]. However, the presence of losses limits their employment in transport applications. In this regard, semiconductor nanowires overcome this issue and allow for a long-range coupling through propagating guided modes, being, in turn, a suitable platform to manage the electromagnetic environment at optical frequencies at the nanoscale [22]. They possess strong optical resonances and/or guided modes that can be richly tuned by their geometrical and/or material properties [22–24]. Nevertheless, they have

been mainly studied as optical cavities [25–28], in which quantum dots or wells are placed inside the nanowire during the growth process, constricting light propagation inside. In fact, to the best of our knowledge, coupling nanowire propagating modes to external excitonic media has not been studied yet; this will presumably have a strong impact on exciton transport applications [29–32].

In the present work, we study theoretically the appearance of strong-coupling regimes in a system consisting of a semiconductor nanowire embedded in an excitonic medium by means of the interplay between guided modes and excitonic states. Upon exploiting the evanescent tail of various weakly guided modes outside the semiconductor nanowire, analyzed in detail through classical electrodynamics (Sec. II), coupling to excitonic modes of an organic dye surrounding the nanowire is plausible. A quantum model is developed to properly determine the polaritonic modes revealed through an avoided crossing with expectedly large enough Rabi splittings (Sec. III), showing that a strong-coupling regime can be accomplished. The distribution of the energy is also affected by the coupling (Sec. IV), going from pure photonic to excitonic states, revealing the hybrid nature of the modes. These entangled modes can be relevant for exciton transport purposes, for which the half-life and propagation length must be optimized (Sec. V).

II. WEAKLY GUIDED SEMICONDUCTOR NANOWIRE MODES

We study the dispersion relation of polaritons arising from the coupling between guided modes in semiconductor nanowires and excitons in a surrounding molecular medium, through both classical and quantum models. We first

discuss the classical electromagnetism approach, which is based on solving Maxwell's equations to obtain guided modes in the system. Here, the molecular medium surrounding the nanowire is modeled through its dielectric function, with excitons manifesting as resonances leading to broad absorption bands. In the second step, we discuss a quantum model in which the guided photonic modes of the semiconductor nanowires are quantized explicitly and coupled to dye molecules modeled as point dipole emitters [19], with a level structure and molecular density that reproduce the classical dielectric function in the (linear) low-excitation limit.

For both procedures, the dispersion relation of the nanowire modes must be solved within classical electromagnetism. Cylindrical waveguides support propagating waves (leaky and guided) with a dispersion relation determined by [23,33]

$$m^2 \frac{(k_z R)^2}{(\omega R/c)^2} = \left[\frac{\mu_c J'_m(u)}{u J_m(u)} - \frac{\mu_b H'_m(v)}{v H_m(v)} \right] \times \left[\frac{\varepsilon_c J'_m(u)}{u J_m(u)} - \frac{\varepsilon_b H'_m(v)}{v H_m(v)} \right], \quad (1)$$

where R is the radius of the cylinder, ω is the angular frequency, k_z is the wave vector of the mode along the cylinder axis, and m is an integer related to the azimuthal distributions of the fields. Furthermore, J_m and H_m are the Bessel and Hankel functions of the first kind, and the prime (') denotes the derivative with respect to the argument. The parameters $u = k_c R$ and $v = k_b R$ are proportional to the transverse component of the wave vector inside and outside the cylinder, respectively, given by

$$k_c^2 = \varepsilon_c \mu_c \frac{\omega^2}{c^2} - k_z^2, \quad (2a)$$

$$k_b^2 = \varepsilon_b \mu_b \frac{\omega^2}{c^2} - k_z^2, \quad (2b)$$

where c is the speed of light in vacuum and ε_c , μ_c and ε_b , μ_b are the electric permittivity and magnetic permeability of the cylinder and background medium, respectively. In the following, we use $\mu_c = \mu_b = 1$.

Recall that Bessel functions are transcendental with a denumerable infinity of roots; thus, for each subindex m in Eq. (1) several solutions are associated that can be denoted by the subscript l . Hence, a pair index ml can be associated with each guided mode. For guided modes with $m = 0$, the field is symmetric about the cylinder axis, exhibiting a pure transverse character, either electric (TE_{0l} , $E_z = E_r = H_\phi = 0$) or magnetic (TM_{0l} , $H_z = H_r = E_\phi = 0$). Hybrid modes arise for $m \neq 0$ (HE_{ml}), where, in general, all field components are nonzero and their phases accumulate a factor of $2\pi m$ in a closed loop around the cylinder axis.

We first consider the "bare" modes of the nanowire embedded in a host material without organic molecules. We consider high-refractive-index, lossless semiconductor nanowires; without loss of generality, a refractive index of $n = \sqrt{\varepsilon_c} = 4.2$ (close to those of GaAs, GaP, and AlSb in the visible spectrum) is used for the nanowire, while the background dielectric constant is set to $\varepsilon_b = \varepsilon_h = 2.4$ (typical for polymers such as polymethyl methacrylate (PMMA)

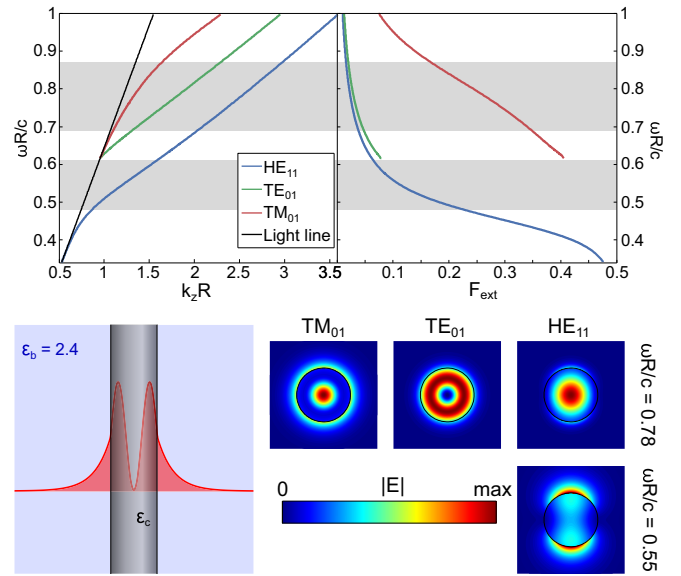


FIG. 1. Bare system. Top: Dispersion relation $\omega R/c$ vs $k_z R$ for the first three guided modes for $\varepsilon_b = 2.4$ and $\varepsilon_c = 4.2^2$. The gray-shaded areas mark the spectral regions that will be studied later. Bottom: Schematic of the waveguide system and norm of the electric field profile of each mode at $\omega R/c = 0.55$ and $\omega R/c = 0.78$.

and polyvinyl acetate (PVAc)). The top left panel of Fig. 1 shows the dispersion relations ($k_z R$ vs $\omega R/c$) of the first three guided modes (HE_{11} , TE_{01} , TM_{01}). In order to optimize the coupling of these modes to molecules that will be placed in the medium surrounding the nanowire, the mode should carry as much energy as possible outside the wire. This implies that the maximum coupling can be achieved with weakly guided modes close to the light line since their field profiles possess large evanescent tails outside the wire. To quantify this, the top right panel of Fig. 1 shows F_{ext} , defined as the fraction of mode energy stored in the electric field outside the nanowire. As the excitonic transitions of dye molecules correspond, to a very good approximation, to electric dipole transitions, only the energy density from the electric field is taken into account. This implies that $F_{\text{ext}} \leq 0.5$ since for guided propagating modes the energy is equally divided between electric and magnetic fields. As can be seen, the cutoff-free HE_{11} mode at lower frequencies and the (predominant) transverse magnetic modes (for dielectric waveguides) close to their cutoff frequencies are both candidates to exhibit strong-coupling phenomenology F_{ext} coming close to its maximum value of 0.5, and both modes become more bounded as the normalized frequency $\omega R/c$ increases. For transverse electric modes, the continuity of all field components across the boundaries causes a flatter dispersion relation and a larger confinement of the field inside the nanowire. As we will see later, strong coupling can still be achieved for TE modes, albeit with smaller Rabi splittings. The bottom of Fig. 1 shows the electric field intensity profiles for each mode at normalized frequencies $\omega R/c = 0.55$ (where only the HE_{11} mode exists) and $\omega R/c = 0.78$, as well a pictorial representation of the system. The field profiles confirm the information for F_{ext} , showing large electromagnetic fields outside the nanowire for the HE_{11} and TM_{01} modes. We note that in the top panels of Fig. 1, the shaded areas mark the

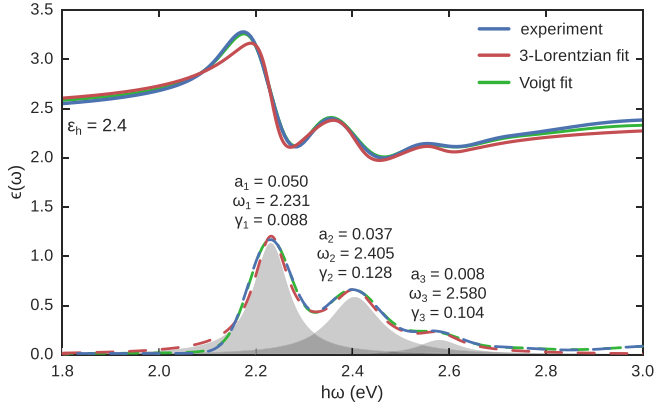


FIG. 2. Experimental value, fit to three Lorentzians and Voigt fit of the dye dielectric function, both real parts (solid curves) and imaginary parts (dashed curves). The shaded areas show the contribution to the imaginary part of each Lorentzian peak. Note that the Lorentzian fit overestimates losses at the low-frequency tail of the first resonance.

spectral regions where the excitonic states are located for nanowire diameters $D = 2R = 90$ nm (bottom shaded area) and $D = 120$ and 130 nm (top shaded area), as will be studied below.

After identifying the suitable bare photonic modes of the system, we now include the effect of an organic dye within the host medium, first staying within a classical description. Without loss of generality, we choose a rylene dye [N,N'-Bis(2,6-diisopropylphenyl)-1,7- and -1,6-bis(2,6-diisopropylphenoxy)-perylene-3,4:9,10-tetracarboximide] as the dye molecule. This molecule has been used in various experiments, achieving strong coupling as it shows little biexciton annihilation even at high densities and is well characterized [34,35]. Its measured electric permittivity (both real and imaginary parts) is shown in Fig. 2 (blue lines), together with a fit to a model dielectric function containing three Lorentzian resonances to represent dye excitations (red lines):

$$\varepsilon(\omega) = \varepsilon_h + \sum_{k=1}^3 \frac{a_k}{\omega_k - i\gamma_k/2 - \omega}, \quad (3)$$

where ε_h is the background permittivity of the host medium and ω_k , γ_k , and a_k are the frequency, decay rate, and amplitude of each resonance, respectively. The fit parameter values are given in Fig. 2 next to each peak. While the fit with Lorentzian resonances is reasonably accurate, we note here that a nearly perfect fit to the dielectric function can be achieved by using Voigt profiles instead of Lorentzian ones. These correspond to the convolution of Lorentzians with Gaussians and can represent both homogeneous and inhomogeneous broadenings, while only homogeneous broadening (i.e., losses and dephasing) is accounted for through Lorentzian profiles.

As the physical results do not change significantly (we have compared both approaches), for simplicity we use the Lorentzian fit to calculate the dispersion relations. However, since Lorentzians have much longer tails than seen in the experimental absorption spectrum, this approximation significantly overestimates the losses at frequencies below about

2.1 eV. As we will see later, using the experimental dielectric function (or, equivalently, the fit to Voigt profiles) leads to significantly longer lifetimes and propagation lengths when strong coupling “pushes” the polaritonic states away from the molecular resonances.

The dispersion relation of the nanowires surrounded by molecules, as calculated within a classical approach by solving Fig. 1, is shown in Fig. 3 for the three first modes (solid curves) and for three different wire diameters, $D = 90, 120, 130$ nm, in order to analyze the coupling to different modes. Here, the dot-dashed curves represent the dispersion relations for the bare system, and the (horizontal) dotted lines represent the resonance frequencies of the excitons. In contrast to the bare-wire case, the lossy nature of the dye resonances implies that the wave vector k_z acquires an imaginary part representing the propagation losses of the polariton modes. The dispersion relations show significant energy shifts close to the resonances of the molecule excitons and also feature a back bending that can indicate a mode hybridization, i.e., strong coupling or polariton formation, in the classical calculations. As expected, the observed splitting is more pronounced for bare photonic modes that are only weakly confined within the nanowire, as well as for dye resonances with larger associated transition dipole moments (i.e., larger absorption amplitude a_n). However, it should be noted that even the more strongly confined TE_{01} mode displays back bending at the first excitonic resonance.

III. QUANTUM MODEL: RABI SPLITTINGS

The classical analysis shows bending bands in the dispersion relation, which are an indicative signature of a strongly coupled system in which avoided crossings arise at resonances. Nonetheless, such behavior could be just the result of the lossy medium itself [36]. In addition, the real coupling is difficult to quantify without a representative quantity such as the Rabi splitting, which has a direct meaning in a quantum description but does not show up explicitly in the classical calculation.

To construct a quantum model, we proceed in a manner similar to that in [19]. We start by quantizing the guided bare-nanowire modes by placing the system within a box of length L along the wire axis and imposing periodic boundary conditions in this direction. This restricts the allowed values of the parallel momentum to $k_z = \frac{2\pi n}{L}$, with $n \in \mathbb{Z}$. Since the bare nanowire modes are lossless and confined in the transverse direction, this also allows for their straightforward quantization by imposing that the integrated energy density is equal to the photon energy (see, e.g., the Appendix of [32]). Defining the quantized field profile $\vec{\mathcal{E}}(\vec{r}) = C\vec{E}(r)e^{ik_z z + im\phi}$ in cylindrical coordinates r, ϕ, z , where $\vec{E}(r)$ is the electric field profile of the mode with arbitrary normalization, gives

$$C = \sqrt{\frac{\hbar\omega}{2\pi LU_{\text{rad}}}}, \quad (4)$$

where U_{rad} is an integral over the electromagnetic energy density of the mode, given by

$$U_{\text{rad}} = 2 \int \varepsilon(r) |\vec{E}(r)|^2 dr. \quad (5)$$

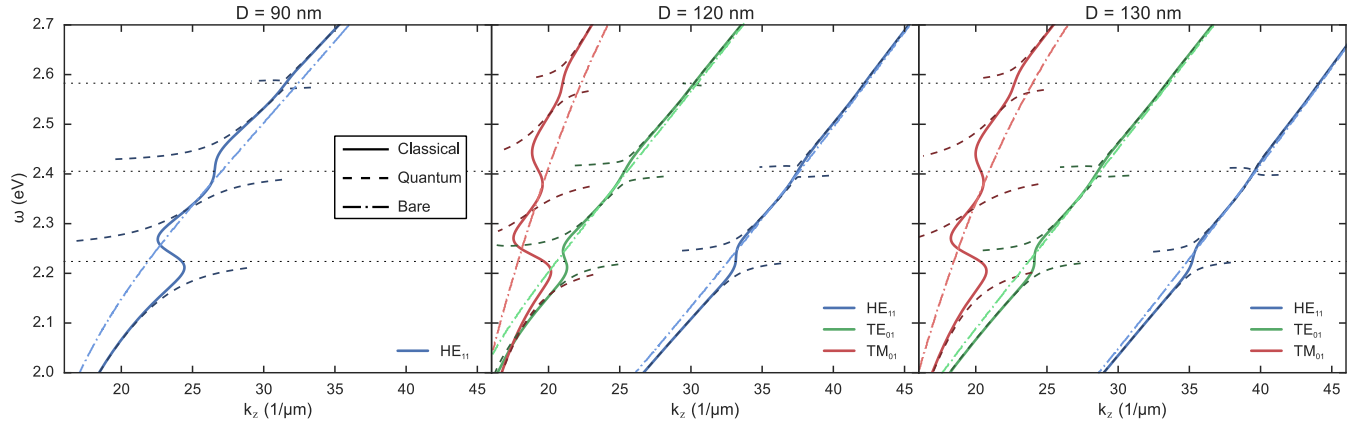


FIG. 3. Comparison between the classical electromagnetics calculation of mode dispersions (solid curves) from Eq. (1) with $\epsilon_c = 4.2^2$ and ϵ_c from the fit to Eq. (3) shown in Fig. 2 and the quantum model (dashed curves), Eq. (14), for three nanowire diameters, $D = 90, 120, 130$ nm. For clarity, only quantum modes with a significant photon fraction are shown (the parts not shown are basically straight lines at the bare emitter frequencies, marked by dotted horizontal lines). For comparison, the bare dispersion relations are shown as dot-dashed curves [Eq. (1) with $\epsilon_c = 4.2^2$ and $\epsilon_c = 2.4$].

Here, the factor of 2 accounts for the fact that equal energy is stored in the magnetic field and in the electric field. Note that we are treating only guided waveguide modes, for which U_{rad} is well defined as k_b is purely imaginary and the mode profile decays exponentially far away from the wire. In addition, there is a continuum of freely propagating modes inside the light cone, which we neglect as they do not play a large role in the situations we study here (although they can have important effects in specific cases [37]). The Hamiltonian of the system within the rotating-wave approximation is then given by

$$H = \sum_{n,m} \omega_{c,nm} \hat{a}_{nm}^\dagger \hat{a}_{nm} + \sum_j H_{\text{mol},j} + \sum_{n,m,j} \vec{\mathcal{E}}_{nm}(\vec{r}_j) \cdot \vec{d}_j (\hat{\rho}_j^- \hat{a}_{nm}^\dagger + \hat{\rho}_j^+ \hat{a}_{nm}), \quad (6)$$

where \hat{a}_{nm} is the bosonic annihilation operator corresponding to the m th mode with parallel momentum $k_z = \frac{2\pi n}{L}$, while $H_{\text{mol},j}$ and $\hat{\rho}_j = \hat{\rho}_j^+ + \hat{\rho}_j^-$ are the bare Hamiltonian and dipole operator of molecule j , respectively, and \vec{d}_j is a unit vector describing the orientation of the molecule. We have here neglected an extra term (proportional to A^2 or $\hat{\rho}^2$, depending on the gauge) in the light-matter interaction which becomes important only in the limit of ultrastrong coupling, i.e., when coupling strengths become comparable to the bare transition frequencies [38–41]. The dye molecules are represented as few-level emitters with parameters chosen to reproduce the macroscopic dielectric function. In particular, we treat the molecules as four-level systems, with one ground and three excited states,

$$H_{\text{mol},j} = \begin{pmatrix} 0 & 0 & 0 & 0 \\ 0 & \omega_1 - i\frac{\gamma_1}{2} & 0 & 0 \\ 0 & 0 & \omega_2 - i\frac{\gamma_2}{2} & 0 \\ 0 & 0 & 0 & \omega_3 - i\frac{\gamma_3}{2} \end{pmatrix}, \quad (7)$$

$$\hat{\rho}_j = \begin{pmatrix} 0 & a_1 & a_2 & a_3 \\ a_1 & 0 & 0 & 0 \\ a_2 & 0 & 0 & 0 \\ a_3 & 0 & 0 & 0 \end{pmatrix}, \quad (8)$$

where the parameters ω_k , γ_k , and a_k are taken from the fit in Eq. (3). Note that we also neglect direct dipole-dipole interactions between the molecules, as their (averaged) effect is already included in the transition frequencies ω_k extracted from the dielectric function. We note for completeness that an alternative (but much costlier) approach would be to extract the molecular parameters from a fit to the bare-molecule polarizability (obtained from the dielectric function using the Clausius-Mossotti relation) and then explicitly include dipole-dipole interactions between the molecules.

We treat the experimentally relevant limit that the host material contains many randomly oriented organic dye molecules, distributed evenly in the region around the nanowire with number density $\rho_{\text{mol}} = 1/V_{\text{mol}}$, where V_{mol} is the average volume occupied by each molecule. Considering the random distribution of the molecules along the wire, translational symmetry is approximately conserved [19], and consequently, superpositions of molecular states can be formed with a well-defined wave vector k_z . The Hamiltonian thus becomes (approximately) diagonal as a function of the parallel wave vector index n , significantly simplifying its diagonalization.

In addition, for the case when more than a single guided mode exists at a given k_z (as is the case for $D = 120$ nm and $D = 130$ nm), we can also approximate that since the nanowire modes are orthogonal, they couple to independent Dicke states (superpositions of molecular excitations). This implies that the coupling between different wire modes and molecular excitations is independent. The collective coupling strength between the i th mode with parallel momentum k_n and the molecular Dicke state corresponding to the k th excitation is then given by

$$g_{nmk}^2 = \sum_j |\vec{\mathcal{E}}_{nm}(\vec{r}_j) \cdot \vec{d}_j a_k|^2. \quad (9)$$

Considering the cylindrical symmetry of the system and that the molecules are randomly oriented and fill all of the space outside the wire evenly, the coupling strength can be

approximated by

$$g_{nmk}^2 \approx \frac{4\pi L}{3} \frac{a_k^2}{V_{\text{mol}}} \int_R^\infty r |\vec{\mathcal{E}}_{nm}(r)|^2 dr. \quad (10)$$

Using Eqs. (4) and (5), the coupling strength can be written as

$$g_{nmk}^2 = \frac{2\hbar\omega_{c,nm}}{3\pi\epsilon_h} \frac{a_k^2}{V_{\text{mol}}} \frac{U_{\text{ext},nm}^{el}}{U_{\text{rad},nm}}, \quad (11)$$

where U_{ext}^{el} is the part of the mode energy stored in the electric field outside the wire,

$$U_{\text{ext}}^{el} = \int_{r>R} \epsilon_h |\vec{\mathcal{E}}(\vec{r})|^2 d\vec{r}. \quad (12)$$

This can be expressed through $F_{\text{ext}} = U_{\text{ext}}^{el}/U_{\text{rad}}$ and the molecular density ρ_{mol} as

$$g_{nmk} = a_k \sqrt{\frac{2\hbar\rho_{\text{mol}}}{3\pi\epsilon_h} \omega_{c,nm} F_{\text{ext},nm}}. \quad (13)$$

It is interesting to note that the coupling strength does not depend on whether the guided nanowire mode has a small mode volume (strong localization of the field). The only information about the wire mode entering the final expression is its frequency and the fraction of the mode energy that is outside the wire. Note that this assumes that space is completely filled with molecules, so that a less confined mode effectively interacts with more molecules to give the same (or even larger) collective coupling as a confined mode. The localization of the mode is compensated by the field strength, and in that sense, well-confined (out-of-the-wire) modes are advantageous only in terms of needing less space and not in terms of reaching strong coupling.

We can now take the limit $L \rightarrow \infty$, such that $k_z = 2\pi n/L$ becomes a continuous variable, and proceed to construct an effective 4×4 model Hamiltonian for each k_z and each nanowire mode independently:

$$H_i(k_z) = \begin{pmatrix} \omega_{c,m}(k_z) & g_{m1}(k_z) & g_{m2}(k_z) & g_{m3}(k_z) \\ g_{m1}(k_z) & \omega_1 - i\frac{\gamma_1}{2} & 0 & 0 \\ g_{m2}(k_z) & 0 & \omega_2 - i\frac{\gamma_2}{2} & 0 \\ g_{m3}(k_z) & 0 & 0 & \omega_3 - i\frac{\gamma_3}{2} \end{pmatrix}, \quad (14)$$

where m labels the nanowire mode and $g_{mk}(k_z)$ is given by Eq. (13).

In Fig. 3, the dispersion relations calculated by the eigenvalues of Eq. (14) are shown (dashed colored curves) with proper avoided crossings appearing near excitonic frequencies manifesting the strong coupling, leading to polaritonic modes. Out of resonance, as expected, the dispersion relations are practically the same as those of the classical bare photonic modes. It should be pointed out that the classical electromagnetic calculations work at real energies ω but allow complex momenta k_z (describing propagation loss). On the other hand, the quantum model works at real k_z but allows complex energies (describing temporal loss). These two pictures represent the same physics but are not completely equivalent. These differences are the reason for the different behaviors close to the regions of largest absorption where the classical modes bend backwards (stationary electromagnetic field solutions), while the quantum modes are actually split (time dynamic driving

process). We also note that the good agreement between quantum and classical calculations in Fig. 3, without any fit parameters, cannot be reproduced by the often-used strategy of constructing an approximate model with k_z -independent couplings g_{mk} (corresponding to approximating $\omega_c F_{\text{ext}}$ as constant).

Furthermore, we emphasize that the quantum model here clearly shows that strong coupling is reached for these conditions. The Rabi splitting Ω_R is estimated from the splitting of the eigenenergies of Eq. (14) at resonance. For example, the cleanest system is given by the nanowire with diameter $D = 90$ nm, for which only the HE_{11} mode is guided. This system supports strong coupling with significant Rabi splittings $\Omega_R > 100$ meV for both the first and second molecular excitations. Moreover, nanowires with larger diameters support multiple polaritons (also with significant Rabi splitting) at the same frequency, which might be interesting for possible applications.

IV. ENERGY DISTRIBUTION: PHOTONIC AND EXCITONIC MODES

An important characteristic of strong coupling is coherent energy exchange between different physical systems, inducing hybrid states that no longer can be seen or described as individual systems. The distribution of the energy into photonic and excitonic parts is important to characterize the new states.

From a classical perspective, the electromagnetic energy for lossy media then can be calculated as a perturbation from the lossless case. However, the strong dispersion and the high losses of the permittivity invalidate the usual expressions for the electromagnetic energy stored in the system. In addition, there is no clear distinction between the energy stored in the medium and that stored in the electromagnetic field. For this purpose, we follow the approach taken by Loudon [42] for the energy of a medium with a single resonant frequency and its extension to multiple resonances [43,44], considering each excitonic state as an independent resonance.

The energy of an absorbing dielectric medium described by resonances is

$$W = W_o + W_f,$$

$$W_o = \frac{1}{4} \int_R^\infty r \epsilon_0 |\vec{E}(\vec{r})|^2 dr \sum_n \frac{2a_n \omega (\omega_n^2 + \omega^2)}{(\omega_n^2 - \omega^2)^2 + \omega^2 \gamma_n^2},$$

$$W_f = \frac{1}{4} \int_0^\infty r [\epsilon_0 \epsilon_r |\vec{E}(\vec{r})|^2 + \mu_0 \mu_r |\vec{H}(\vec{r})|^2] dr, \quad (15)$$

where

$$\epsilon_r = \begin{cases} \epsilon_c, & r < R, \\ \epsilon_h, & r > R, \end{cases} \quad \mu_r = \begin{cases} \mu_c, & r < R, \\ \mu_b, & r > R. \end{cases} \quad (16)$$

The first term of Eq. (15), W_o , is the energy stored in the excited oscillators (excitons), and it goes to zero out of the resonances. The second term, W_f , is the energy carried by the electromagnetic field.

Within the quantum model, the excitonic energy is calculated as the (real part of the) expectation value of the molecular exciton Hamiltonian H_{mol} in each state, relative to the total energy of the eigenstate.

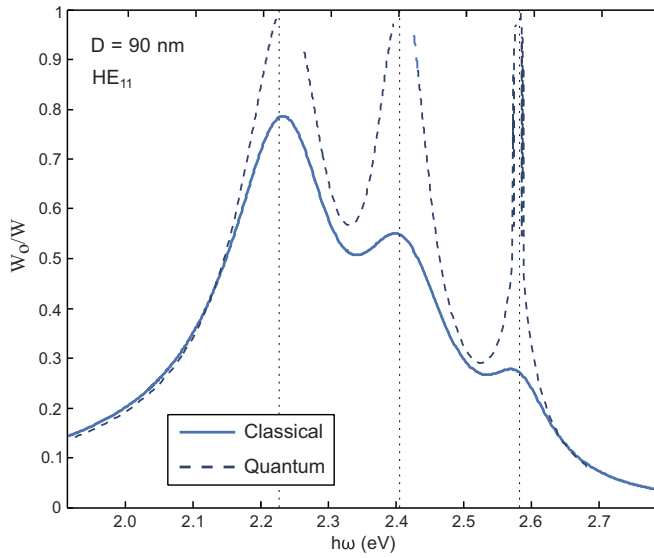


FIG. 4. Fraction of the energy stored in the excitons calculated by the classical (solid curve) and quantum approach (dashed curve) for the HE_{11} mode at a nanowire diameter of $D = 90$ nm. The material properties are the same as in Fig. 3. The resonant frequencies of the excitons are marked by dotted vertical lines.

As we have previously seen that each nanowire mode is independent from the point of view of the coupling with the excitonic media, we now focus only on the case $D = 90$ nm (results for other modes are analogous). The ratio between the energy stored in the oscillators and the total energy of the system, $W = W_o + W_f$, characterizes the nature of the mode (photonic/excitonic). Figure 4 shows the percentage of the energy stored in the excitons obtained by the classical (solid curve) and quantum approaches (dashed curve) for the HE_{11} mode at $D = 90$ nm. The agreement between both approaches is extremely good at the frequencies where both dispersion relations coincide (see Fig. 3). Far from resonance, the energy stored in the oscillators goes to zero; thus, there is no interaction with the excitons, and the mode is practically photonic. In the spectral region of the resonance bands, the fraction of the energy in the excitons increases, as the mode becomes polaritonic. Close to resonance, as expected from the differences in the dispersion relation, the approaches differ: whereas the energy fraction within the classical model yields smooth maximal values (below 100%) at the excitonic frequencies (corresponding to the regions in which the mode dispersion relation bends backwards in Fig. 3), the quantum approach asymptotically tends to 1, namely, to 100% of energy stored as excitons (flat dispersion relation in Fig. 3).

It is interesting to note that a high enough fraction of excitonic energy is required for this system to be a suitable platform for excitonic applications; however, at the same time, it is desirable to minimize losses, which is achieved for high photon components. A good compromise can be achieved at intermediate-energy fractions below the onset of losses in the dielectric function ($h\omega \approx 2.1$ eV, at which $W_o/W \approx 0.3$), as we will show below.

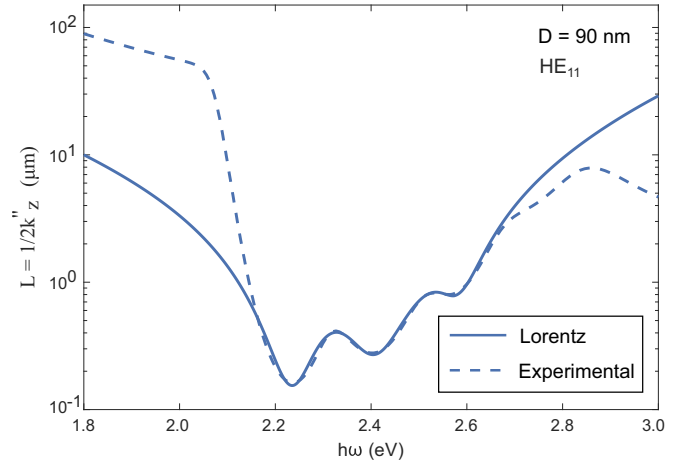


FIG. 5. Classical calculations of the propagation length L_p (in logarithmic scale) as a function of frequency for the HE_{11} mode ($D = 90$ nm). Solid curve: the dielectric function is fitted to a Lorentzian model (Fig. 2). Dashed curve: the experimental value of the dielectric function is used.

V. HALF-LIFE, PROPAGATION LENGTH, AND ENERGY VELOCITY

While, up to now, we have focused on the real part of the quantities (wave vectors and/or energies), the losses of the system are also a very important part necessary to obtain a complete characterization. In particular, they determine dynamic properties such as the mode propagation length that are crucial for practical applications. Thus far, we have studied the properties of the system using a Lorentzian fit for the dielectric function, rather than the experimentally measured one, since this allows more direct comparison with a simple quantum model and gives almost identical results for the dispersion relation and allows us to determine the existence of strong coupling. However, the Lorentzian fit severely overestimates losses away from the resonances, and much more reliable results are obtained when using the actual experimental values in order to calculate properties such as the half-life τ and the propagation length L_p (linked through the group velocity v_g).

The propagation length L_p is the distance after which the energy of the wave is reduced to $1/e$ of its initial value. For the classical approach, the propagation length of a guided mode is given by $L_p = 1/2k_z''$, inversely proportional to the imaginary part of the propagation constant, $k_z = k_z' + ik_z''$, that accounts for the attenuation of the mode. In Fig. 5 the propagation length of the HE_{11} mode for $D = 90$ nm (as in Fig. 4) is plotted in logarithmic scale as a function of the frequency using both the experimental value of the dielectric function and the Lorentzian fit from Eq. (3) shown in Fig. 2.

At frequencies below first resonance, L_p using the experimental dielectric function gives values that are typically one order of magnitude larger than with the Lorentzian fit and gives propagation lengths that are one to two orders of magnitude larger than the wavelength of the mode.

We also note that the difference between dielectric functions is much smaller for the TE_{01} and TM_{01} modes at very low frequencies (not shown here). This is due to the fact

that, as the modes become leaky, the radiation processes begin to dominate losses and the imaginary part of the permittivity is no longer determinant. On the other hand, as expected, both methods give similar results at frequencies close to resonance (2.2–2.6 eV), where the Lorentzian fits accurately reproduce the dielectric function. Finally, the Lorentzian fit leads to higher (unphysical) values of L_p at high frequencies since another resonance appears that was not included in the fit therein.

For current and future applications that rely on exciton transport [29–31,45], large propagation lengths are desired while simultaneously keeping a considerable amount of energy in the excitons (excited oscillators). To achieve better coupling, the mode energy must be outside the wire, although the localization of the energy in the excitonic medium would imply higher losses. These two issues must be balanced in order to optimize the propagation length. An important effect to take into account here is that the propagation length is determined by the dielectric losses at the frequency of the polariton mode. This implies that strong coupling can be used to push the exciton peak away from the exciton losses through polariton formation, allowing us to create states with high exciton character that do not suffer from the large excitonic losses. This is a particular strength of the semiconductor nanowire systems studied here, where the bare photonic modes are essentially lossless. For example, focusing on the HE_{11} mode and demanding that 30% of the energy be in the excitons, the maximum propagation length is reached at a diameter $D = 70$ nm, with $L_p = 48 \mu\text{m}$ at $h\omega = 2.02$ eV (at the lower part of the first resonant frequency). The propagation wavelength of the mode at that frequency is 367 nm, 130 times smaller than the propagation length. As a general consideration, the propagation length is optimal (related to the energy stored in the excitonic media) close to frequencies at which losses start to substantially increase due to inhomogeneous broadening.

The velocity at which energy is transported by a propagating mode is normally given by the group velocity v_g , defined as

$$v_g = \frac{d\omega}{dk}. \quad (17)$$

However, the velocity at which the energy is transported must always be lower than the speed of light, which is not fulfilled by this definition; for example, in the region where the photonic bands bend backward, the group velocity goes to infinity. Therefore, as for the energy, an alternative definition is needed in lossy media. Following the works of Loudon and Brillouin [42,46], we define the energy velocity v_e as the ratio between the flow of energy, given by the Poynting vector, and the total energy stored in the system,

$$v_e = \frac{S_z}{W} = \frac{\int_0^\infty r S_z(\vec{r}) dr}{W}. \quad (18)$$

For the bare photonic states calculated before (the lossless case), the results given by Eqs. (16) and (17) are identical (not shown here).

In Fig. 6 the energy velocity (divided by the speed of light in the host medium c_h) of the HE_{11} mode is shown for $D = 90$ nm. In addition, the result for the bare system

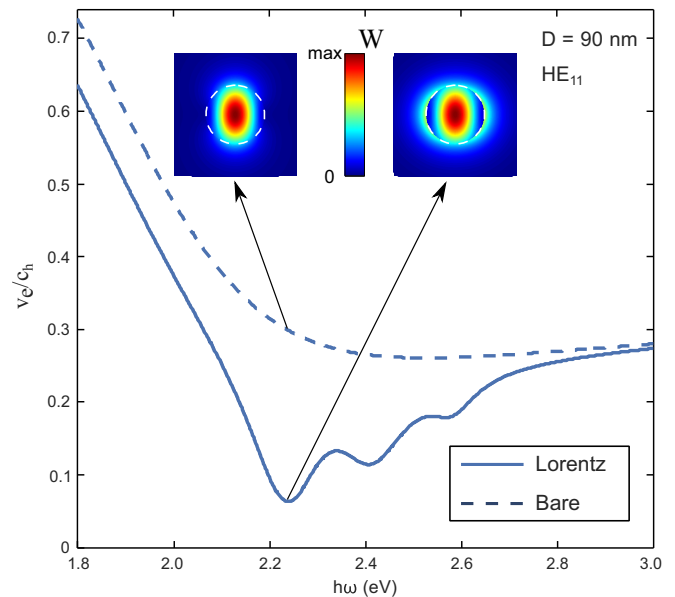


FIG. 6. Classical calculations of the energy velocity v_e divided by the speed of light in the host medium c_h as a function of frequency for the HE_{11} mode ($D = 90$ nm). Solid curve: dielectric function fitted to a Lorentzian model; dashed curve: bare system ($\epsilon_b = 2.4$). The insets show the energy distribution at the first resonant frequency $h\omega = 2.23$ eV for both cases.

is also included (dashed line). The energy velocity presents dips at resonant frequencies. Strong coupling manifests as a reduction in the energy velocity since the coherent exchange of energy slows down the light flow. At resonant frequencies, the electric permittivity of the excitonic media matches the value of the background ϵ_b . Despite the nonzero imaginary part, the field profiles for both cases (with and without resonances) are very similar, and so are the value of the Poynting vector and the energy inside the wire. However, the energy outside the wire presents an additional contribution W_o due to the excitons (see insets in Fig. 6), slowing the propagation of the energy down.

VI. CONCLUDING REMARKS

In conclusion, we have shown that strong coupling between weakly guided modes of a semiconductor nanowire and a surrounding excitonic medium can be achieved, exhibiting Rabi splittings of more than $\Omega_R > 100$ meV for an organic dye. The bare photonic modes are determined through a rigorous classical analysis, namely, waveguide propagating modes with an evanescent tail outside the nanowire. The evanescent tail allows for strong coupling of the nanowire modes with the excitons in external dye molecules. The underlying physical mechanism is similar to surface plasmon polaritons in metallic nanorods, but with the advantage of much larger propagating lengths due to the nearly complete absence of absorption inside the semiconductor nanowire. A quantum model provides a straightforward analytical expression for the Rabi splitting and reveals that the relevant quantity is not the field concentration but the fraction of the field interacting with the emitters. The quantum model also

reveals that coherent energy exchange plays an important role in the coupled system: the dispersion relations reveal avoided crossings with clear Rabi splittings, as expected from strong coupling. We furthermore showed that the polariton modes in these systems can achieve significant propagation lengths up to two orders of magnitude larger than the bare mode wavelengths while still maintaining a significant excitonic character. This happens because strong coupling can shift exciton modes to frequency regions where material losses are much smaller than around the exciton resonances. Recalling that lowest-order nanowire guided modes can be considered nearly one-dimensional lossless propagating modes [24], we thus anticipate that the proposed configuration might be a suitable candidate for enhanced exciton conductance [31], which

holds promise for applications related to exciton transport, slow light, and conversion modes.

ACKNOWLEDGMENTS

The authors acknowledge the Spanish Ministerio de Economía, Industria y Competitividad for financial support through Grants No. MAT2014-53432-C5-5-R, No. FIS2015-69295-C3-2-P, and No. FIS2017-91413-EXP; the María de Maeztu program for Units of Excellence in R&D (MDM-2014-0377); and an FPU Fellowship (D.R.A.) and a Ramón y Cajal grant (J.F.). We also acknowledge funding from the European Research Council (ERC-2016-STG-714870).

-
- [1] J. A. Hutchison, A. Liscio, T. Schwartz, A. Canaguier-Durand, C. Genet, V. Palermo, P. Samorì, and T. W. Ebbesen, *Adv. Mater.* **25**, 2481 (2013).
- [2] S. Ghosh, W. H. Wang, F. M. Mendoza, R. C. Myers, X. Li, N. Samarth, A. C. Gossard, and D. D. Awschalom, *Nat. Mater.* **5**, 261 (2006).
- [3] L. Novotny, *Am. J. Phys.* **78**, 1199 (2010).
- [4] L. C. Andreani, G. Panzarini, and J.-M. Gérard, *Phys. Rev. B* **60**, 13276 (1999).
- [5] Y. Zhu, D. J. Gauthier, S. E. Morin, Q. Wu, H. J. Carmichael, and T. W. Mossberg, *Phys. Rev. Lett.* **64**, 2499 (1990).
- [6] G. Khitrova, H. M. Gibbs, M. Kira, S. W. Koch, and A. Scherer, *Nat. Phys.* **2**, 81 (2006).
- [7] S. Haroche and D. Kleppner, *Phys. Today* **42**(1), 24 (1989).
- [8] T. H. Taminiau, F. D. Stefani, and N. F. van Hulst, *Opt. Express* **16**, 10858 (2008).
- [9] S. Kühn, U. Håkanson, L. Rogobete, and V. Sandoghdar, *Phys. Rev. Lett.* **97**, 017402 (2006).
- [10] E. Yablonovitch, *J. Opt. Soc. Am. B* **10**, 283 (1993).
- [11] A. Wallraff, D. I. Schuster, A. Blais, L. Frunzio, R.-S. Huang, J. Majer, S. Kumar, S. M. Girvin, and R. J. Schoelkopf, *Nature* **431**, 162 (2004).
- [12] S. R. K. Rodriguez, Y. T. Chen, T. P. Steinbusch, M. A. Verschuuren, A. F. Koenderink, and J. G. Rivas, *Phys. Rev. B* **90**, 235406 (2014).
- [13] S. R. K. Rodriguez, J. Feist, M. A. Verschuuren, F. J. García Vidal, and J. Gómez Rivas, *Phys. Rev. Lett.* **111**, 166802 (2013).
- [14] S. Wang, S. Li, T. Chervy, A. Shalabney, S. Azzini, E. Orgiu, J. A. Hutchison, C. Genet, P. Samorì, and T. W. Ebbesen, *Nano Lett.* **16**, 4368 (2016).
- [15] I. Pockrand, A. Brillante, and D. Möbius, *J. Chem. Phys.* **77**, 6289 (1982).
- [16] R. Houdré, R. P. Stanley, and M. Ilegems, *Phys. Rev. A* **53**, 2711 (1996).
- [17] J. Bellessa, C. Bonnand, J. C. Plenet, and J. Mugnier, *Phys. Rev. Lett.* **93**, 036404 (2004).
- [18] J. Bellessa, C. Symonds, K. Vynck, A. Lemaitre, A. Brioude, L. Beaur, J. C. Plenet, P. Viste, D. Felbacq, E. Cambriil, and P. Valvin, *Phys. Rev. B* **80**, 033303 (2009).
- [19] A. González-Tudela, P. A. Huidobro, L. Martín-Moreno, C. Tejedor, and F. J. García-Vidal, *Phys. Rev. Lett.* **110**, 126801 (2013).
- [20] L. Shi, T. K. Hakala, H. T. Rekola, J.-P. Martikainen, R. J. Moerland, and P. Törmä, *Phys. Rev. Lett.* **112**, 153002 (2014).
- [21] P. Törmä and W. L. Barnes, *Rep. Prog. Phys.* **78**, 013901 (2015).
- [22] R. Yan, D. Gargas, and P. Yang, *Nat. Photonics* **3**, 569 (2009).
- [23] D. R. Abujetas, R. Paniagua-Domínguez, and J. A. Sánchez-Gil, *ACS Photonics* **2**, 921 (2015).
- [24] R. Paniagua-Domínguez, G. Grzela, J. G. Rivas, and J. A. Sánchez-Gil, *Nanoscale* **5**, 10582 (2013).
- [25] J. P. Reithmaier, G. Sek, A. Löffler, C. Hofmann, S. Kuhn, S. Reitzenstein, L. V. Keldysh, V. D. Kulakovskii, T. L. Reinecke, and A. Forchel, *Nature* **432**, 197 (2004).
- [26] K. Hennessy, A. Badolato, M. Winger, D. Gerace, M. Atatüre, S. Gulde, S. Fält, E. L. Hu, and A. Imamoglu, *Nature* **445**, 896 (2007).
- [27] L. K. van Vugt, B. Piccione, C.-h. Cho, P. Nukala, and R. Agarwal, *Proc. Natl. Acad. Sci. USA* **108**, 10050 (2011).
- [28] K. Kuruma, Y. Ota, M. Kakuda, D. Takamiya, S. Iwamoto, and Y. Arakawa, *Appl. Phys. Lett.* **109**, 071110 (2016).
- [29] A. A. High, E. E. Novitskaya, L. V. Butov, M. Hanson, and A. C. Gossard, *Science* **321**, 229 (2008).
- [30] S. M. Menke, W. A. Luhman, and R. J. Holmes, *Nat. Mater.* **12**, 152 (2012).
- [31] J. Feist and F. J. Garcia-Vidal, *Phys. Rev. Lett.* **114**, 196402 (2015).
- [32] C. Gonzalez-Ballester, J. Feist, E. Moreno, and F. J. Garcia-Vidal, *Phys. Rev. B* **92**, 121402(R) (2015).
- [33] J. A. Stratton, *Electromagnetic Theory* (McGraw-Hill, New York, 1941).
- [34] M. Ramezani, A. Halpin, A. I. Fernández-Domínguez, J. Feist, S. R.-K. Rodriguez, F. J. Garcia-Vidal, and J. Gómez Rivas, *Optica* **4**, 31 (2017).
- [35] M. Ramezani, A. Halpin, J. Feist, N. Van Hoof, A. I. Fernández-Domínguez, F. J. Garcia-Vidal, and J. Gómez Rivas, *ACS Photonics* **5**, 233 (2018).
- [36] C. Wolff, K. Busch, and N. A. Mortensen, *Phys. Rev. B* **97**, 104203 (2018).

- [37] J. Yuen-Zhou, S. K. Saikin, and V. M. Menon, *J. Phys. Chem. Lett.* **9**, 6511 (2018).
- [38] C. Ciuti and I. Carusotto, *Phys. Rev. A* **74**, 033811 (2006).
- [39] S. De Liberato, *Nat. Commun.* **8**, 1465 (2017).
- [40] D. De Bernardis, T. Jaako, and P. Rabl, *Phys. Rev. A* **97**, 043820 (2018).
- [41] C. Schäfer, M. Ruggenthaler, and A. Rubio, *Phys. Rev. A* **98**, 043801 (2018).
- [42] R. Loudon, *J. Phys. A* **3**, 233 (1970).
- [43] K. E. Oughstun and S. Shen, *J. Opt. Soc. Am. B* **5**, 2395 (1988).
- [44] J. E. Vázquez-Lozano and A. Martínez, *Phys. Rev. Lett.* **121**, 043901 (2018).
- [45] D. Ballarini, M. De Giorgi, E. Cancellieri, R. Houdré, E. Giacobino, R. Cingolani, A. Bramati, G. Gigli, and D. Sanvitto, *Nat. Commun.* **4**, 1778 (2013).
- [46] L. Brillouin, *Wave Propagation and Group Velocity* (Academic, New York, 1960).